Computers & Fluids 53 (2012) 1–14

Contents lists available at SciVerse ScienceDirect

Computers & Fluids

journal homepage: www.elsevier.com/locate/compfluid

Nonlinear identification of unsteady heat transfer of a cylinder in pulsating cross flow

F. Selimefendigil, S. Föller, W. Polifke *

Lehrstuhl für Thermodynamik, TU München, Garching 85747, Germany

ARTICLE INFO

Article history:
Received 4 August 2009
Received in revised form 13 June 2011
Accepted 18 August 2011
Available online 5 October 2011

Keywords:
Nonlinear system identification
Higher order transfer functions
Describing function
Thermoacoustic system
Convective heat transfer
Pulsating flow

ABSTRACT

Unsteady heat transfer of a cylinder in pulsating cross flow is investigated. The heat transfer process is considered as a nonlinear single-input, single-output system, with large amplitude velocity perturbations as "input" and total heat transfer rate from the cylinder surface to the fluid as "output". Quantitatively accurate, low-order models of the heat source dynamics are obtained with a variety of nonlinear system identification methods from time series data generated with unsteady CFD computations. A polynomial type, equation error identification scheme is found to yield very accurate results. In order to obtain the heat source response function in the frequency domain, the equation error model is converted into the frequency domain using harmonic balance as well as harmonic probing approaches. In the harmonic balance approach, a set of nonlinear algebraic equations is solved for the coefficients of the harmonic ansatz. In the harmonic probing method, a recursive relation is obtained to deliver the higher order transfer functions of the nonlinear heat source. Alternatively, a nonlinear black box identification technique is used to identify the heat source dynamics. It is found to capture the amplitudes of higher harmonics with increased accuracy.

1. Introduction

Feedback coupling between acoustics and heat release within a thermoacoustic device or combustor may result in self-excited instability. In combustors, thermoacoustic instabilities are associated with excessive noise emissions, structural damage and inefficient operating conditions [12,30,39]. Prediction and control of thermoacoustic instabilities is thus an important design objective.

The growth of linearly unstable modes is in general limited by nonlinearities, resulting in the formation of the steady state, periodic oscillations ("limit cycles"). The detrimental effects of instabilities on combustor life time and noise emissions depend on the limit cycle amplitudes. Furthermore, linearly stable modes may go nonlinearly unstable in response to finite amplitude perturbations. Clearly, nonlinear effects are important for thermoacoustic stability and limit cycle amplitudes, thus their analysis and prediction is important [47].

In thermoacoustic systems, either gas dynamics or the behavior of the heat source may give rise to nonlinear effects. Gas dynamics nonlinearity – e.g. wave steepening – is of primary importance in rocket engines, where pressure fluctuation amplitudes reach 20–50% of the mean. Culick and co-workers [37,55] have considered second and third order nonlinearity for gas dynamics in combustion chambers. Approximate solutions based on a modal expansion approach ("spatial averaging") were developed and used to analyze the existence and the stability of limit cycles.

In premixed combustion instability, on the other hand, the nonlinearity associated with the response of the heat source to velocity perturbations is often the dominant nonlinear effect. Indeed, in many premixed combustors the magnitude of pressure fluctuations at the onset of the nonlinearity is quite small. Reported pressure amplitudes are of the order of 1–5% of the mean [25]. Thus a linear treatment of acoustic wave propagation is usually considered adequate, while it is crucial to have an accurate, nonlinear dynamic model of the relationship between flow in the vicinity of the heat source and the heat release.

In this context, the "flame describing function" – an amplitude dependent frequency response of a nonlinear element to sinusoidal input – has received considerable attention [11,13,16,45,48]. Noiray et al. [33] applied a nonlinear extension of the well-known network model approach (see below) to a premix burner. This method, which includes a flame describing function as essential nonlinear element, predicted thermoacoustic limit cycles and other nonlinear effects like hysteresis with good accuracy.

In the present paper, nonlinear methods of system identification (SI) based on time series data generated with computational fluid dynamics are used to describe the behavior of a nonlinear heat source. The resulting models are "richer" than the describing

* Corresponding author.
E-mail addresses: fthsel@yahoo.com (F. Selimefendigil), foeller@td.mw.tum.de (S. Föller), polifke@td.mw.tum.de (W. Polifke).

0045-7930/$ - see front matter © 2011 Elsevier Ltd. All rights reserved.
doi:10.1016/j.compfluid.2011.08.012

function, as they do account, e.g. for nonlinear modal coupling [46,47]. At the same time, the describing function may by computed from the SI-based models in an efficient manner, and indeed in the present work, validation of the nonlinear system identification results makes use of the describing function (see below).

The methods presented are based on time series data and thus in principle applicable to a wide variety of heat sources – in particular laminar or even turbulent flames. In this study, however, only the wire gauze in a Rijke tube is considered as a model heat source, since the basic physics of this configuration is well understood and it has adequate nonlinearity even at relatively small fluctuation amplitudes. This eases the analysis of the system for implementation and validation of the various nonlinear identification strategies.

The paper is organized as follows: firstly, some background on linear and nonlinear stability analysis for thermoacoustic systems is provided, previous work on heat transfer in pulsating flows is reviewed. Then the computational fluid dynamics (CFD) model for heat transfer of a cylinder in pulsating cross flow, which is to represent the wire gauze in a Rijke tube, is described. CFD results for the describing function, computed with Fast Fourier Transformation (FFT) from the response to sinusoidal forcing are presented next. In the following sections, basics of system identification are reviewed and the equations for a second order polynomial identification using an equation error type model structure are presented. The identification method is extended into the frequency domain using two different approaches, namely, a harmonic balance approach and a harmonic probing approach. In the former case, a system of equations for the coefficients of the harmonic ansatz, and in the latter case, a recursive relation to compute the higher order transfer functions is obtained. Lastly, a nonlinear black box approach is used to identify the heat source. Validation is based on results for the describing function where appropriate, the respective strengths and deficiencies of the various SI methods are discussed.

2. Background

In this section, pertinent background information on linear as well as nonlinear stability analysis for thermoacoustic systems is provided. Also, previous work on the dynamics of heat transfer in pulsating flow is reviewed briefly.

2.1. Linear and nonlinear stability analysis

Prediction of thermoacoustic stability limits and limit cycle amplitudes requires suitable models for acoustic wave propagation and dissipation as well as an adequate model for the heat source, valid in the nonlinear regime. In principle, CFD computation of the full thermoacoustic system with a compressible flow model could provide all required information. However, such computations generally demand huge computational resources, since thermoacoustic instabilities involve various physical phenomena covering a wide range of length and time scales [39,53]. Considering that during development of a combustion system, the dependency of stability characteristics on various parameters has to be checked, one must conclude that the straightforward CFD modeling of thermoacoustic instability is unfeasible for design purposes.

Linearization of the Navier–Stokes equation yields the inhomogeneous wave equation for pressure fluctuations with a source term, which represents the heat release rate from combustion [32,36,53]. The inhomogeneous wave equation can be solved in the time- or frequency domain with a finite element of finite volume approach, if a suitable model for the source term is provided, e.g. in the form of an $n-\tau$ model or generalizations thereof [32,36].

Alternatively, an approximate solution of the inhomogeneous wave equation can be obtained by a modal expansion method ("Galerkin method") [9,10,56]. In the Galerkin method, acoustic variables are expressed in terms of basis functions, which satisfy the boundary conditions and constitute a complete basis. Again, a model for the heat source must be provided as input to the method. If this sub-model has many delay terms, numerical integration of the resulting delay differential system may be computationally expensive. Note that both the inhomogeneous wave equation and the Galerkin method can predict limit cycle amplitudes.

Low-order "network models" are attractive since they are very flexible and require solving a set of algebraic equations instead of partial differential equations, see e.g. [39] and references therein. In this approach, individual elements of a thermoacoustic system are described by their respective transfer or scattering matrix. Information on the dynamics of the heat source is usually provided in the form of a flame transfer or describing function. Linear network models based on the transfer function can predict the frequency and the growth rate of eigenmodes, an extension to the nonlinear regime was achieved with the describing function method [11,33]. Even if the input to the heat source (usually the only nonlinear element) is assumed to be sinusoidal, the nonlinear effects will produce higher harmonics, which are at multiple integers of the fundamental frequency. The describing function method neglects the effect of coupling between modes, since it is a one-mode (sinusoid) approximation. If the flame response or the system acoustic filters the higher harmonics, a good approximation for limit cycle behavior is possible.

With the exception of the "brute force" CFD method, all approaches for thermoacoustic stability and limit cycle analysis require information on the dynamics of the heat source. In the context of the present paper, it is emphasized that a sub-model for the heat source is suitable for our purposes only if it is able to predict the fluctuating heat release rate in response to a variety of velocity perturbation signals, rather than merely the "training" time series data that were used to identify the model. In particular, since the frequencies of unstable eigenmodes or limit cycle amplitudes are in general not known a priori, the heat release sub-model should be valid for a wide range of frequencies and amplitudes.

2.2. Heat transfer in pulsating flow

Empirical correlations, which relate incoming velocity perturbations to the heat transfer rate, have been proposed for the wire mesh of a Rijke tube. Well known and widely used in hot wire anemometry is "King's Law" [19],

$$Q(t) = L_w(T_w - T)\left(\lambda_a + 2\sqrt{\pi\lambda_a c_v \bar{\rho}\frac{d_w}{2}|u(t-\tau)|}\right). \tag{1}$$

Material properties of the fluid are denoted by $\bar{\rho}$ for the mean density, c_v for the specific heat at constant volume, and λ_a for the heat conductivity of fluid. L_w and d_w represent the length and the diameter of the wire, respectively. T_w is the temperature of the wire, and τ is the time lag.

For small velocity fluctuations, the heat transfer rate has a linear dependence upon the fluctuation amplitude. This can be explicated by rewriting Eq. (1) as,

$$Q'(t) + \overline{Q} = K_1 + K_2\sqrt{\left|1 + \frac{u'(t-\tau)}{\bar{u}}\right|}, \tag{2}$$

where K_1 and K_2 are constants defined as,

$$K_1 = L_w(T_w - T)\lambda_a, \quad K_2 = 2L_w(T_w - T)\sqrt{\pi\lambda_a c_v \bar{\rho}\frac{d_w}{2\bar{u}}}.$$

For fluctuation amplitude u' much less than the mean velocity $\bar{u}$, a Taylor series approximation for the square-root nonlinearity is written as,

$$\sqrt{\left|1+\frac{u'(t-\tau)}{\bar{u}}\right|}=1+\frac{1}{2}\frac{u'(t-\tau)}{\bar{u}}-\frac{1}{8}\left(\frac{u'(t-\tau)}{\bar{u}}\right)^2+\cdots. \quad (3)$$

Neglecting the higher order terms, a linearized form of King's Law is obtained,

$$Q'(t)=\frac{K_2}{2}\frac{u'(t-\tau)}{\bar{u}}, \quad (4)$$

which is equivalent to the "$n-\tau$" formulation of a thermoacoustic heat source [30]. Note that this correlation assumes only a single time lag between the incoming perturbation velocity u' and the heat transfer rate fluctuation Q'.

Alternatively, thermal boundary layer response to periodic outer flow may be calculated analytically using perturbation or averaging techniques [26,27,52]. In these methods, an analytical closed form representation can be obtained for low amplitudes of fluctuation in the limit of high and low frequencies, respectively. One may also consider nonlinear contributions in the boundary layer response [52]. In that case, higher harmonics as well as nonlinear streaming effects appear in the thermal and hydrodynamic boundary layer responses. Some physical insight can be obtained from this treatment for the phase relation between the fluctuations of velocity and heat transfer rate.

Nonlinear effects in a Rijke tube (a resonator tube configuration with a velocity sensitive heat source) were analyzed numerically and experimentally by Heckl [18]. For the heat source, a modified version of King's law was proposed, with a square-root type nonlinearity that sets in at approximately 30% amplitudes. It was shown by Heckl that with increasing amplitudes, nonlinearity in the heat source determines the saturation of the instability. Matveev [29] derived a nonlinear transfer function model of the heat source in a Rijke tube, using convective heat transfer equation in unsteady flow. A quasi-steady approach was used, and the amplitude dependence of the phase of the transfer function was taken into account. The heat source model in that study is very similar to the one used by Heckl [18]. It was shown that flow reversal at the heat source is critical for the nonlinearity in heat transfer.

3. CFD model of heat transfer in pulsating flow

Hantschk and Vortmeyer [17] performed numerical simulation of self-excited thermoacoustic instability in a Rijke tube. The compressible Navier–Stokes and energy equations were solved in a two dimensional domain with open or closed acoustic boundary conditions. Heating strips kept at constant temperature were used as heating elements. Due to limited computational resources, flow and heat transfer at the heater was not fully resolved. Instead, wall temperature and thermal conductivity were set to unphysical, high values in order to have sufficient heat transfer to the gas. Frequencies and limit cycle amplitudes of unstable modes were identified in qualitative agreement with experiment. It was found that flow reversal in the vicinity of the heat source is responsible for nonlinear effects, which are observed at velocity fluctuation amplitudes as low as 30% of the mean in agreement with Heckl's finding [18].

The dynamics of fluctuating heat transfer in pulsating flow was investigated neither in detail nor with quantitative accuracy by Hantschk and Vortmeyer [17]. This is one of the objectives of the present study, thus a high resolution CFD model representing only one wire of the heater gauze in a Rijke tube was set up, see Fig. 1. The corresponding cylinder in cross flow configuration is shown in Fig. 2.

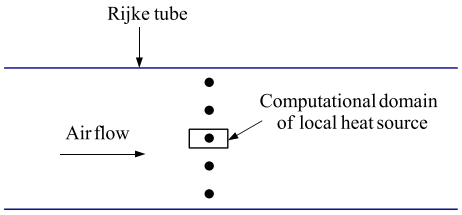

Fig. 1. Schematic of a Rijke tube with a wire gauze as heat source.

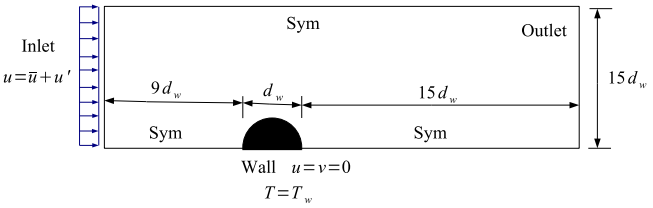

Fig. 2. Geometry and boundary conditions for CFD modeling of half of a single wire.

Table 1
Property values of air used in CFD computations.

Property	Units	Value
Density	kg/m^3	1.164
Specific heat capacity	J/kg − K	1005
Thermal conductivity	W/m − K	0.0026
Dynamic viscosity	kg/m s	1.848e−5

At the inlet and outlet, "velocity inlet" and "pressure outlet" boundary conditions are imposed, respectively. The property values of the fluid (air) used in the CFD computations are presented in Table 1. The mean flow Reynolds number based on wire diameter $d_w = 10^{-3}$ m, $\mathrm{Re} \equiv \rho \bar{u} d_w/\mu$, where $\bar{u}, \rho$ and μ represent the mean velocity, density and dynamic viscosity of the flow, respectively, is an important parameter. Karman vortex streets are observed downstream of a cylinder at Reynolds number Re > 40. In the present case Re = 13, thus Karman vortices are absent and the use of symmetry boundary conditions at the top and bottom of the domain to reduce the size of the computational domain is thus justified. The vertical component of the velocity vanishes ($v = 0$) at the symmetry boundaries. On the cylinder surface, wall boundary conditions with zero velocities ($u = v = 0$) and constant temperature ($T = T_w$) were imposed. The body-fitted mesh is composed of 16,540 quadrilateral elements and is refined close to the cylinder surface. Mesh independence of the solutions was confirmed.

The unsteady, incompressible Navier–Stokes equation along with the energy equation is solved with FLUENT 6.1 segregated solver (a general purpose finite volume solver) [14]. The use of an incompressible flow model is justified, because acoustic wave lengths considered are much larger than the wire diameter d_w, i.e. the heat source is "acoustically compact". The harmonic perturbation at the inlet is transmitted immediately to the outer flow near the cylinder because of the incompressibility assumption. A second order implicit formulation in time, with a time step of 10^{-4} s and a second order accurate spatial discretization are used. Second order upwind schemes are used for the momentum and the energy equations. The global convergence for the continuity, momentum and energy residuals are set to 10^{-4}, 10^{-5} and 10^{-5}. Fluid properties are chosen to be temperature independent.

In the following, some results obtained with harmonic perturbation of the inlet velocity, $u(t) = \bar{u} + u' \sin(\omega t)$ are presented. Forcing amplitude and frequency are characterized by a non-dimensional velocity amplitude ratio (A) and Strouhal Number (Str),

$$A \equiv \frac{u'}{\bar{u}}, \tag{5}$$

$$\mathrm{Str} \equiv \frac{\omega\, d_w}{\bar{u}}. \tag{6}$$

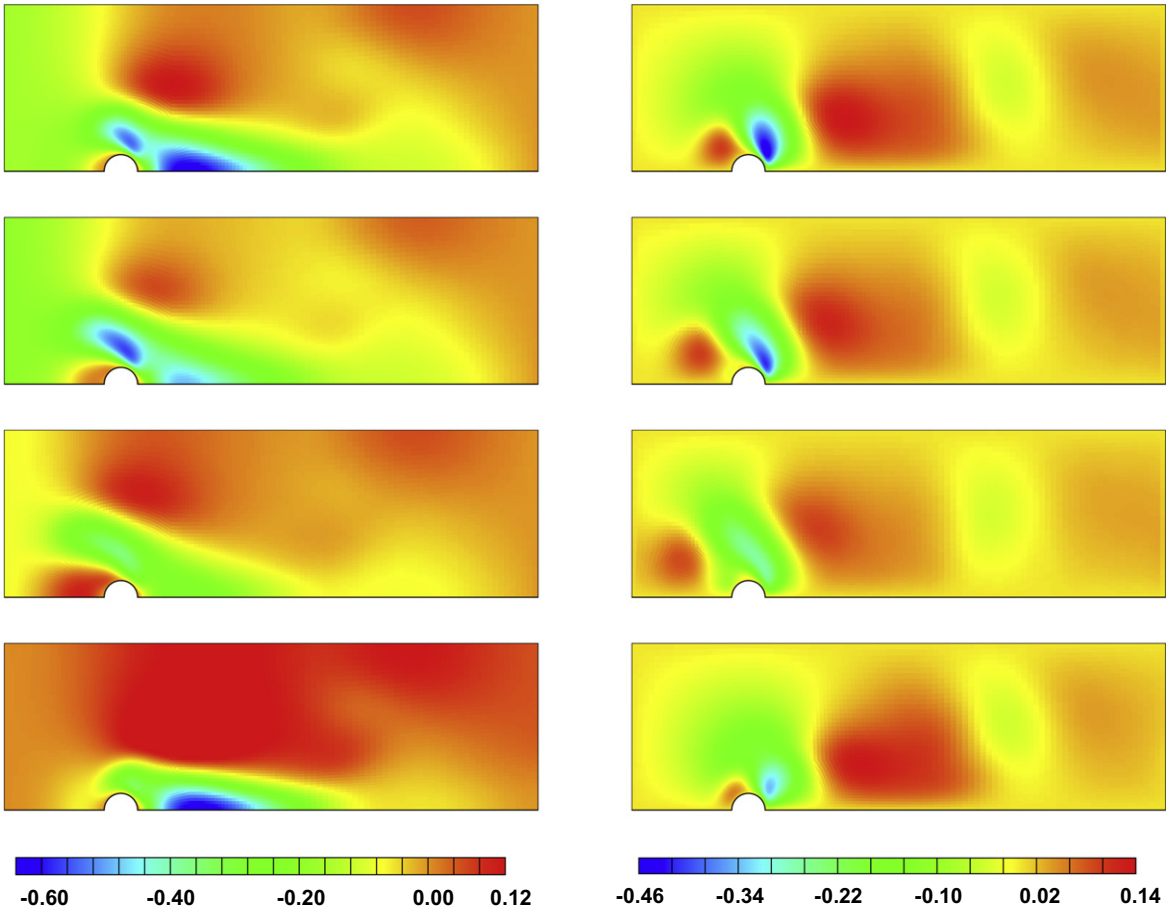

Fig. 3. Velocities at times $t = 0.12566$ s, $t = 0.12880$ s, $t = 0.13194$ s, $t = 0.15393$ s from top to bottom with period $T = 0.0314$ s. Left: u-velocity. Right: v-velocity.

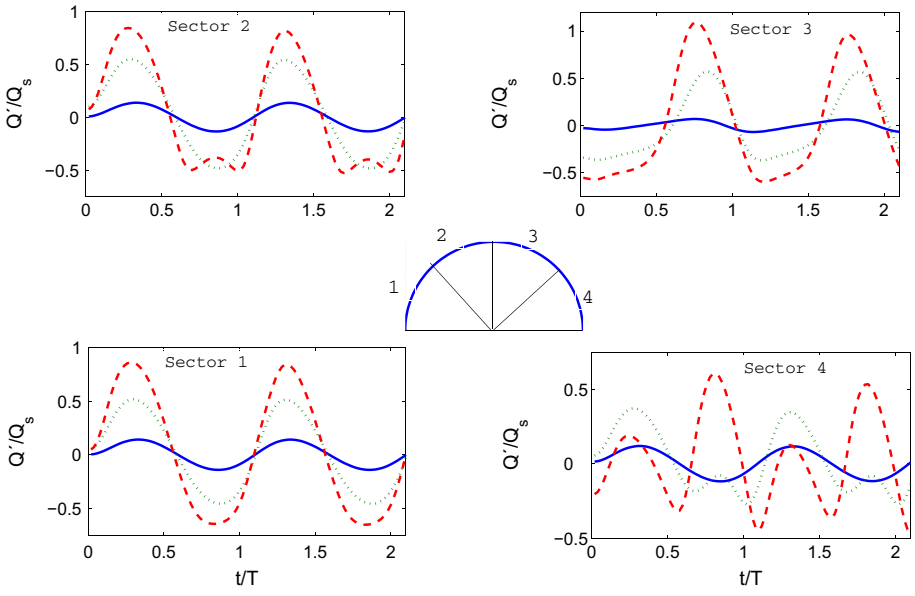

Fig. 4. Normalized heat transfer rate for forcing amplitudes $A = 2$ (dashed lines), $A = 1$ (dotted lines) and $A = 0.3$ (continuous lines) at Strouhal number Str = 0.361. Results for sectors 1–4 of the cylinder surface are shown in sub-plots clockwise from bottom-left to bottom-right.

Some snapshots of velocity distributions are shown in Fig. 3 for different time instances within one period, for velocity amplitude ratio $A = 2$ and Strouhal number of Str = 0.361. The first three sub-figures of Fig. 3 from top, show the velocities when outflow occurs at the inlet boundary due to high pulsation amplitude. For the inflow boundary (left edge of the domain), this situation requires no special treatment; the prescribed velocity is imposed even if it is negative. For the outflow boundary (right edge of the domain) the "backflow" option of the CFD solver imposes a "pressure inlet" condition, provided that "incoming" values for temperature, etc., are prescribed by the user. Because the length of the computational domain is much larger than the maximal displacement of fluid elements, inflow at the right edge of the domain does not affect the heat transfer at the cylinder surface.

Heat flux at the cylinder surface is computed according to Fourier's Law from the wall-normal temperature gradient in the fluid,

$$q_W = -\lambda_a \left.\frac{\partial T}{\partial n}\right|_W, \tag{7}$$

where the subscript "W" indicates that heat flux and temperature gradient are evaluated at the wall. In the numerical simulation, the evaluation of the temperature gradient at the wall is based on the wall neighboring control volume.

Heat transfer is monitored over four sectors of the cylinder surface as indicated in Fig. 4. The wall heat transfer rate per unit width Q (units W/m) is computed as the integral of the wall heat flux q_W over the individual sectors. Fluctuating heat transfer rates (Q') normalized with respect to steady state values (Q_s) are shown for three

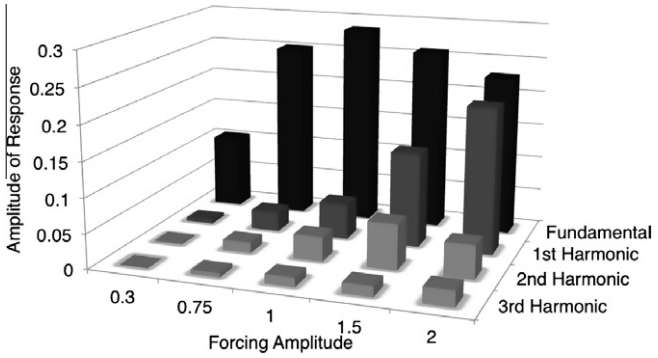

Fig. 5. Absolute value of FFT of fluctuating heat transfer rates for forcing at Str = 0.361 with relative amplitudes $A = 0.3$, 0.75, 1, 1.5 and 2 (corresponding to different shades of gray). Shown is the response at the fundamental and first few harmonic frequencies.

different fluctuating amplitudes in Fig. 4. In these plots, time is normalized with respect to the period of the excitation T. Most of the heat transfer takes place in the first quadrant (bottom-left sub-plot). For low amplitude perturbations $A = 0.3$ almost linear behavior (pure sinusoid) is seen at every sector. For $A = 1$ and $A = 2$, nonlinear contributions are clearly visible, especially in sectors 3 and 4. In agreement with earlier studies [17,18], the following explanation for the nonlinear effects is offered: At large amplitudes, the flow reverses during the second half of the period, resulting in reduced temperature difference from the surface to the flow and thus reduces the effective heat transfer rate from the cylinder.

4. Sinusoidal describing function

From time series data as shown in Fig. 4, the transfer function or – for the nonlinear case – the describing function for the dynamics of the heat source may be computed. Indeed, Föller et al. [15] have obtained the linear transfer function of a heated cylinder in pulsating cross-flow with correlation-based, linear system identification. In the nonlinear regime, a nonlinear description of heat source dynamics can be determined from either single frequency sinusoidal forcing or nonlinear system identification methods. Before exploring the latter in the remainder of this paper, some results for the sinusoidal describing function are presented in this section.

To capture the nonlinearity in the heat transfer, the response to harmonic excitation at different frequencies and amplitudes is determined (by computation or experiment). Fast Fourier Transformation (FFT) of the time series then gives the describing function – an amplitude-dependent, nonlinear extension of the transfer function [16] – at the forcing frequency ω and amplitude A,

$$F(A,\omega) = \left.\frac{\mathrm{FFT}(Q'/Q_s)}{\mathrm{FFT}(u'/u_s)}\right|_{A,\omega}, \tag{8}$$

Computations are performed for discrete amplitudes and frequencies, intermediate values may be obtained by interpolation. Such a heat source model, which is nonlinear through its explicit amplitude dependence, may be used in a frequency domain thermoacoustic system model [11,13].

Some results for the present configuration are presented in Figs. 5 and 6. The response in heat transfer rate to harmonic forcing for a variety of frequencies (Str = 0.361, 1.08, 1.80 and 3.61) and amplitudes ($A = 0.3$, 0.75, 1, 1.5 and 2) are obtained. FFT yields the describing function, i.e. the amplitude ratio and phase relation

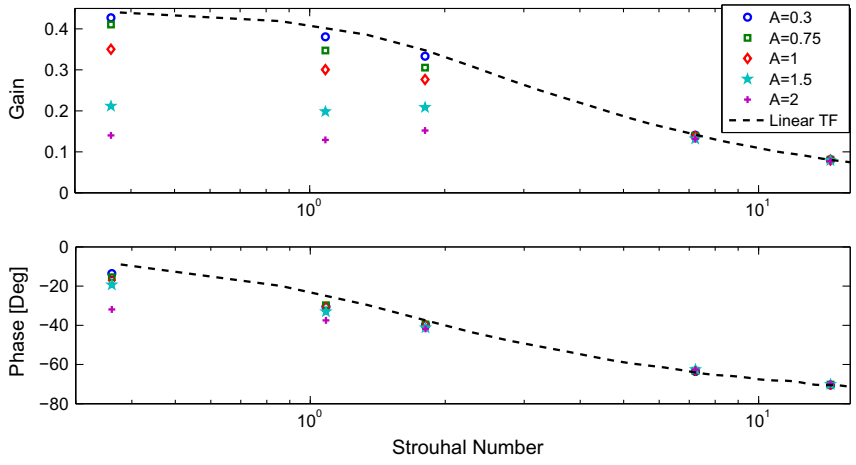

Fig. 6. Gain and phase of the describing function for forcing with single sinusoids at different velocity amplitude ratios and Strouhal numbers along with a linear transfer function obtained from linear identification on a semi-logarithmic plot.

between the unsteady heat transfer rate and the unsteady velocity at the respective forcing frequency. In Fig. 5, it is seen that the peaks at the integer multiples of the fundamental harmonic increase with fluctuation amplitude. For $A = 2$, the second harmonic reaches nearly 80% of the amplitude of the fundamental.

In Fig. 6, the describing function $F(A, \omega)$ for various amplitude ratios A is shown along with a linear transfer function computed by Föller et al.[15]. At $A = 0.3$, the behavior is linear. The deviation from the linear transfer function is more pronounced at low Strouhal numbers and high velocity amplitude ratios. At higher frequencies, the response approaches linear transfer behavior, a decrease in the gain and an asymptotic value of -70 deg in the phase. Gain is more sensitive than the phase, and indeed the phase dependence on amplitude can be neglected up to $A = 1.5$. Another observation is the non-monotonic behavior of the gain with frequency for $A = 2$, where a decrease in the gain is followed by an increase and then a decrease. Clearly, a large number of CFD computations would be required to cover the relevant range of dynamics with adequate resolution in A and Str. Another disadvantage of the describing function approach is that the response is considered only at the forcing frequency. But in the nonlinear modeling of system behavior, it is also important to consider the higher harmonics. Drawbacks of the FFT approach can be circumvented with nonlinear system identification methods which will be discussed in the following sections. The results presented in this section, forced at specific values of amplitude A and frequency Str, will then serve as a reference to check the validity of nonlinear identification methods.

5. System identification

System identification can be used to construct dynamic models from input–output data sets that may be obtained from an experimental test rig or numerical simulation [28,50]. Polifke and coworkers have used linear system identification methods as an effective tool to construct aero- and thermoacoustic transfer functions/matrices using input–output data sets generated with unsteady CFD, see [41,43] and references therein. With a broadband excitation signal and correlation-based linear identification, one can obtain the transfer function over a wide range of frequencies with moderate computational effort. For the wire heat source considered in this paper, the linear transfer function was identified by Föller et al. [15]. Also, the complex interactions in the hydrodynamic and thermal boundary layers were investigated.

Correlation-based methods assume that the superposition principle holds, and thus cannot be used to identify nonlinear behavior. Schemes for nonlinear system identification will be introduced and applied to the heat transfer in pulsating flow in this section.

5.1. Procedures and model structures used in system identification

Identification methods can generally be classified as parametric and nonparametric. In the parametric approaches, the system is described with differential/difference equations, and the aim is to find the parameters of this mathematical description. Well known nonparametric representations are the *Impulse Response* (in the time domain) and the *Frequency Response* (in the frequency domain).

The input–output representation of an LTI (Linear Time Invariant) system in polynomial form is expressed as [28]:

$$A(z)Q(t) = \frac{B(z)}{F(z)}u(t) + \frac{C(z)}{D(z)}v(t), \tag{9}$$

where A, B, C, D, F are polynomials in terms of z, u and Q are the input and output of the system, and v is the error term. z is a shift operator namely,

$$zQ(t) = Q(t+1). \tag{10}$$

Here, $Q(t+1)$ is a shorthand notation for $Q(t+\Delta t)$, for the time step Δt. This operator simply shifts one step ahead value of the input or output to the current time. The delayed samples of input $(u(t-1), \ldots, u(t-N_u))$ and output $(Q(t-1), \ldots, Q(t-N_Q))$ are called the *regressors*. Depending on the polynomials used, different model structures are known [28], which are briefly introduced here;

- **FIR** (Finite Impulse Response):

  $$A = C = D = F = 1.$$

  This is the simplest model structure to be considered. The past inputs are used as regressors. The structure results in a linear least square problem for minimizing the cost function (e.g. Euclidean norm of the residual between the actual and the estimated output). It requires many regressors and the convergence rate is slow.
- **ARX** (Auto Regressive with eXogenous input):

  $$C = D = F = 1.$$

  This model structure uses the past inputs and past outputs as regressors. This again results in linear least square description where the cost function needs to be minimized.
- **ARMAX** (Auto Regressive Moving Average with eXogenous input):

  $$D = F = 1.$$

- **OE** (Output Error):

  $$A = C = D = 1.$$

For identification, a model structure is selected and the number of past inputs and outputs are specified. Another classification that is important (for an application in "divide and conquer") is based on whether the simulated or measured past outputs are used as regressors in the model structure. In an output error type modeling approach, the simulated past outputs obtained from the model structure are used, whereas, in an equation error type modeling approach, the measured past outputs are used as regressors. A criterion to minimize the difference between the actual output and output from identification are specified in order to get the parameters of the model structures. In an equation error/output error type modeling approach, this criterion results in a linear/nonlinear least square fit.

Identification methods have the following procedures in common [28,42,49,50]:

- **An appropriate choice of the input signal**: The system is excited with a proper signal for the excitation of all relevant modes of interest. Generally, broadband forcing, chirp signals or pseudo random binary sequences, which have white noise characteristics, are used to excite the system for a wide range of frequencies.
- **Model structure selection**: Equation error or output error model structures are used.
- **Selection of the number of past inputs and outputs used in the model structure (the system "memory")**: Depending on the maximum frequencies of interest and the time lag of the system under consideration, the number of regressors is specified. A priori information about the maximum time lag deduced from system physics is in general helpful [42].
- **An algorithm to minimize the cost function**: The difference between responses of the time series data generated from numerical simulation or experiment and identification is minimized. Marquardt–Levenberg algorithm, Gauss–Newton methods or other nonlinear optimization (genetic algorithms, particle swarm optimization) methods are used.

- **Model validation**: The identified model is tested against signals which have not been used in the estimation. In a broadband forcing, half of the data is used for the fit (minimization of the cost function) while the other half is used for validation.

5.2. Nonlinear identification problem

Input–output modeling of the nonlinear systems are generally categorized as nonparametric – functional series expansion (Volterra, Wiener series expansion) – and parametric (differential/difference equation models, neural network models, polynomial models) [4,35]. A Volterra series – a Taylor series expansion of functionals – may be considered as an extension of the impulse response of the linear system to the nonlinear case [5,44]. Orthogonalization of the Volterra series has been proposed to express the input–output modeling of the nonlinear system with reduced number of parameters and to obtain the parameters of the nonlinearity using broadband type excitation signals [20,23]. In Hammerstein and Wiener identification methods, a linear dynamic block is connected to a static nonlinear input and/or output block structure [4,21]. A neural network is a black-box identification method, which uses expansion functions through the so-called "units" (or "layers") to model a nonlinear input–output relation [31,34,38,49]. There also exist local linear models that use fuzzy based algorithms, which could be utilized as nonlinear identification tools [1,2,51].

The procedures and requirements used in nonlinear system identification are comparable to those of linear system identification. The input signal covers the relevant range of frequencies, as well as amplitudes. In order to achieve better convergence rates and/or a smaller number of regressors, it is common to add past outputs in the regressor set. Either the actual outputs, or the computed outputs are then used in the set of regressors. A schematic representation of the corresponding equation error and output error type model structures is shown in Fig. 7. In the figure, z represents the shift operator, which simply shifts the one step ahead value of the input or output to the current time.

If actual output Q is used, an analytical closed form solution for the model parameters is obtained. Also, extension into the frequency domain is fairly straightforward (see below). However, the requirement for actual output limits the range of applications of equation error models. Thus output error models based on computed output Q_m might seem to be the method of choice for a time domain thermoacoustic system model. However, obtaining a model with this identification may be difficult due to stability and nonlinear optimization problems (optimum initial guess, trapping into local minimum). Again, details are discussed in the following.

A nonlinear dynamic fit is generally expressed as

$$Q(t) = F(Q(t-1), \ldots, Q(t-N_Q), u(t), \ldots, u(t-N_u)). \tag{11}$$

For a linear system, the function F is linear with respect to its arguments, i.e. the regressors, $Q(t-i)$, $u(t-j)$. In linear identification, it is therefore comparatively easy to obtain a dynamic model using one of the existing model structures and an appropriate choice of excitation signal. For a nonlinear system, the form of the function F is not known a priori. This function is approximated using expansion functions and polynomials. One can encounter the problem of the "curse of dimensionality" (a significant amount of increase in the parameters by adding extra dimensions corresponding to the degree of nonlinearity and the number of regressors) depending on the maximum time lag of the system, relevant maximum and minimum frequencies and the degree of the nonlinearity. Nonlinear extensions of the linear model structures are named as NFIR, NARX and NARMAX, and NOE [8].

In the time domain modeling of complete thermoacoustic systems, equation error type model structures for the heat source are useless since they require actual outputs for the set of regressor (delayed samples of input and output). Output error models, which make use of outputs from the model, may lead to instability and typical problems of the nonlinear optimization (optimum initial guess, trapping into local minimum). In this study, an equation error type model for a parametrization of the input–output modeling with the polynomials up to second order is considered. The approach is extended into the frequency domain with two different approaches; with a harmonic balance approach and a harmonic probing approach, which provides the nonlinear transfer function and higher order transfer function of the heat source. These nonlinear transfer functions are used to describe the heat source in the frequency domain for a range of operating conditions. They could be used for a frequency domain thermoacoustic system model to account for the coupling of the higher order harmonics with the higher order transfer functions for accurate prediction of the limit cycle amplitudes.

5.3. Polynomial identification

5.3.1. Mathematical formulation

The first identification method discussed is the second order polynomial identification which is of type NARX. It utilizes past

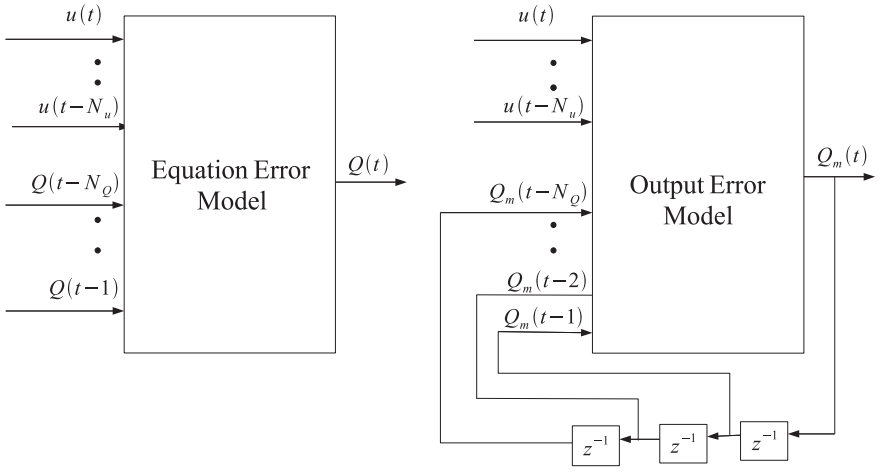

Fig. 7. Schematic of the equation error (left) and output error (right) model structures using actual output Q or computed output Q_m as regressors.

inputs and actual outputs, and considers nonlinear terms up to second order in the regressor set, i.e. the bilinear products of uu and uQ,

$$Q(t) = Q_{\text{approx}}(t) + v(t). \tag{12}$$

The approximated output Q_{approx} is a second order polynomial,

$$\begin{aligned} Q_{\text{approx}}(t) = &\sum_{k=1}^{N_u} h_u(k)u(t-k+1) + \sum_{l=1}^{N_Q} h_Q(l)Q(t-l) \\ &+ \sum_{k=1}^{N_u}\sum_{l=1}^{N_Q} h_{uQ}(k,l)u(t-k+1)Q(t-l) \\ &+ \sum_{k=1}^{N_u}\sum_{m=1}^{N_u} h_{uu}(k,m)u(t-k+1)u(t-m+1). \end{aligned} \tag{13}$$

Here, Q_{approx} and Q represent the approximated and actual output, respectively. The matrix of inputs U, vector of unknown parameters P and regressor set Z are defined as,

$$\begin{aligned} U = [&u(t-k+1), \quad Q(t-l), \quad u(t-k+1)u(t-m+1), \\ &u(t-k+1)Q(t-l)], \end{aligned} \tag{14}$$

$$P = [h_u(k), \quad h_Q(l), \quad h_{uu}(k,m), \quad h_{uQ}(k,l)], \tag{15}$$

$$Z^M = [u(t-k+1), Q(t-l)], \tag{16}$$

$$k,m = 1,\ldots,N_u, \quad l = 1,\ldots,N_Q.$$

The difference (error) between the approximated and actual outputs is minimized in a least square sense

$$V(Z^M;P) = \frac{1}{M}\sum_{i=1}^{M}(Q - PU)^2, \tag{17}$$

where i is a time index. The vector of the unknown parameters is derived from

$$\frac{\partial V}{\partial P} = 0, \quad \text{with} \quad P = \frac{1}{M}\sum_{i=1}^{M}(QU^T)\frac{1}{M}\sum_{i=1}^{M}(UU^T)^{-1}. \tag{18}$$

Since the actual outputs are used in the regressor set, an analytical closed form solution for the unknown parameters P is obtained. This simply represents the product of the cross correlation between the input matrix U and output vector Q, and the inverse of autocorrelation of the input matrix U.

5.3.2. Identification of unsteady heat transfer from unsteady CFD

The CFD model for the heat transfer of the wire in pulsating flow that has been described in the previous chapters is excited with a broadband forcing at the inlet position. In order to excite the nonlinearity in the heat transfer rate of the wire, $A = 2$ is chosen as the perturbation amplitude. The unsteady CFD is calculated for $M = 10{,}000$ time steps with a time step of $\Delta t = 10^{-4}$ s. This time step corresponds to the time step of the CFD computation. Indeed, one may also consider to create input–output data set using integer multiples of CFD samples at equal intervals ($2\Delta t_{CFD}$, $4\Delta t_{CFD}$, $6\Delta t_{CFD}$, etc. or $5\Delta t_{CFD}$, $10\Delta t_{CFD}$, $15\Delta t_{CFD}$,etc.) [40]. Half of the data is used for estimation and the other half is used for validation. Validation is also performed against single frequencies at various amplitudes. A schematic representation for the identification of the heat source using time series generated by unsteady CFD computations is shown in Fig. 8. The parameters of the nonlinearity (when the response from the heat source is parametrized in terms of the delayed samples of inputs and outputs) describes the heat source for a range of amplitudes and frequencies of the pulsating velocity.

The information about the time lag is got from system identification methods. For accurate identification in the linear regime, maximum filter length is chosen to exceed all time delays of the system [42]. The estimation of the order of the time lag in the linear regime, which has been given by Lighthill [26] is rewritten as,

$$\tau = 0.2\frac{d_w}{\bar{u}}, \qquad f \ll 20\frac{\bar{u}}{d_w}. \tag{19}$$

In our case, this corresponds to a time lag of $\tau = 7.2 \times 10^{-4}$ s for frequencies $f \ll 5544$ Hz (with the characteristic length -wire diameter $d_w = 10^{-3}$ m, and mean velocity $\bar{u} = 0.2772$ m/s). This time lag for the linear system is used as an initial option while choosing the filter lengths (number of past inputs and outputs in the regressor set) for nonlinear system identification.

The parameters that are chosen in the second order polynomial identification are N_u and N_Q, which correspond to the maximum time lag in the input and output data, respectively. Also the time lag between the input and the output is selected to be different from zero. If only inputs are used in the identification (NFIR model structure), then a memory filter length of at least 10 is required, according to the time lag of the linear system and the time step of the unsteady CFD computations. On the other hand, if output is used as regressor in the model structure, the memory length may be reduced. In the present case, parameters $N_u = 4$, $N_Q = 3$ are chosen.

A measure of the quality of identification is the match between the output Q_{pred} predicted by the dynamic model and the actual output Q computed with CFD:

$$\text{Fit} = \left[1 - \sqrt{\frac{\sum_{k=1}^{N}\left(Q(k) - Q(k)_{\text{pred}}\right)^2}{\sum_{k=1}^{N}Q(k)^2}}\right] \times 100. \tag{20}$$

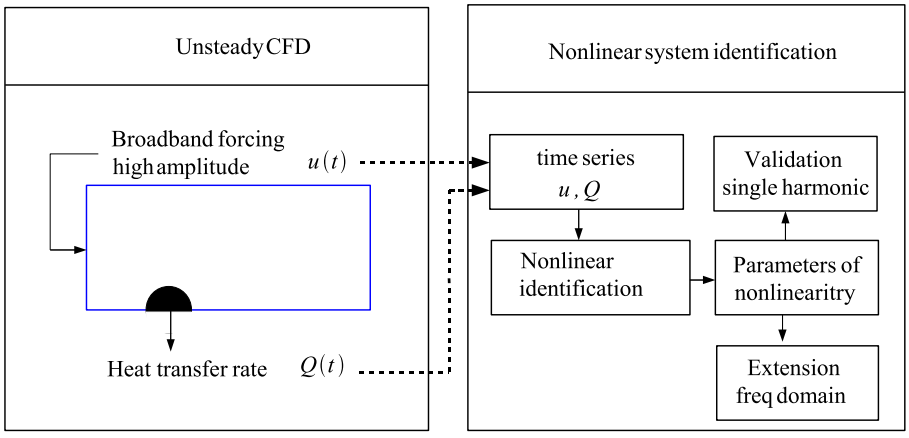

Fig. 8. Schematic of the nonlinear identification from input–output data set of unsteady CFD computation in order to obtain a dynamic model of a heat source.

The fit of the validated model for the second half of the data is 98.15. A segment of time series data is shown in Fig. 9, showing that the quality of the fit is indeed very high.

5.3.3. Validation for single harmonics

The parameters obtained from the polynomial identification with broadband forcing should describe the dynamics of the heat source for a range of amplitudes and frequencies. To check this, validation is performed against CFD data for a single harmonic at different amplitudes. Fast Fourier Transformations of the heat transfer rates from the CFD and from the identified model are shown for Str = 1.805 in Fig. 10 on a single plot for $A = 1.5$ and $A = 2$. The percentage of the error in the amplitude of fundamental peak never exceeds 1%, but for second harmonic it is in the level of up to 5% for Str = 0.361 and Str = 1.807. At Str = 7.229, it exceeds 10%. This is caused by the time step that is used in CFD. In the single harmonic forcing corresponding to Str = 7.229, 1/50 of the period is used as time step, which is less than the time step for the identification with broadband forcing. The results are interpolated from a fine time interval grid to a coarse one. This explains there is a slight difference at high Str. Distortions from the ellipses in the phase portraits are interpreted as indication of the nonlinearity in the heat transfer rate. As seen in Fig. 11, there is a slight difference at $A = 2$ for Str = 1.805 in the phase portraits.

The accuracy of the equation error type identification is very high for the configuration considered. However, the set of regressors requires actual outputs Q (which must be generated, for example, with a CFD model of the wire heat source). It is important to realize that therefore this nonlinear heat source model cannot be used for time domain simulation of a thermoacoustic system, because for such a setup the needed actual output data is not known.

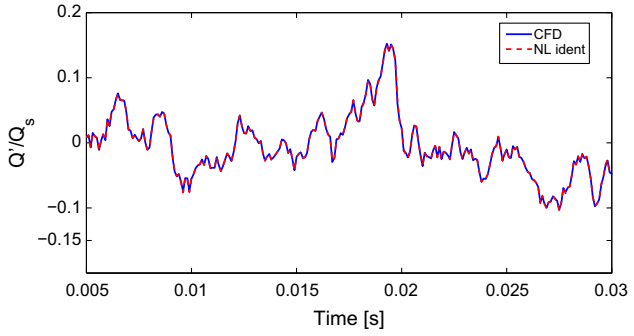

Fig. 9. The degree of the fit between the CFD data (validation data set) and nonlinear system identification, $N_u = 4$, $N_Q = 3$.

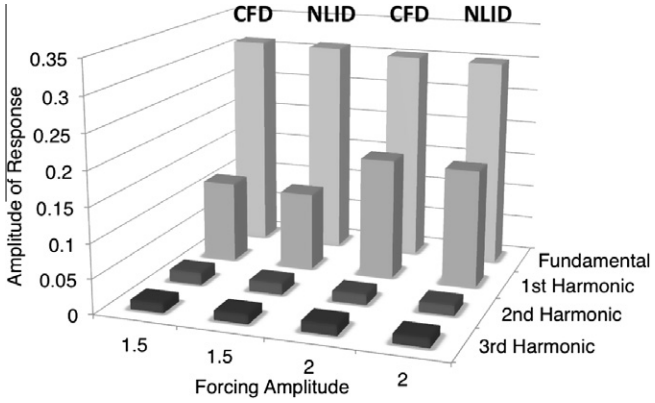

Fig. 10. Comparison of CFD results vs. nonlinear identification: absolute value of FFT of heat transfer rate for forcing amplitudes $A = 1.5$ and $A = 2$ at Str = 1.805. Shown is the response at the fundamental and first few harmonic frequencies.

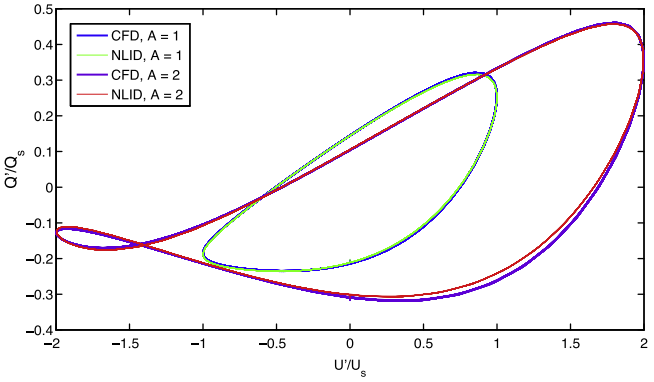

Fig. 11. Comparison of phase portraits computed with CFD vs. nonlinear identification at Str = 1.805 for forcing amplitudes $A = 1$ and $A = 2$, respectively.

Identification procedures suitable for that purpose must be based on NFIR or NOE model structures. NFIR requires only delayed samples of input, NOE requires both delayed samples of input and delayed samples of model output from the identified heat source.

Nevertheless, the advantages of accuracy and ease of use of the equation error type identification scheme can be used in extending it into the frequency domain. Two different approaches, namely, a harmonic balance method and a harmonic probing method are considered next.

5.3.4. Harmonic balance

Let us assume a sinusoidal input to the heat source,

$$u(t) = \frac{U_0}{2i}\left(e^{i\omega t} - e^{-i\omega t}\right), \tag{21}$$

and as the output consider harmonics up to second order;

$$Q(t) = Q_0 + \frac{Q_1}{2}e^{i\omega t} + \frac{Q_{-1}}{2}e^{-i\omega t} + \frac{Q_2}{2}e^{2i\omega t} + \frac{Q_{-2}}{2}e^{-2i\omega t}, \tag{22}$$

where Q_1,Q_{-1}, and Q_2,Q_{-2} are complex conjugate coefficients. The input and output will be replaced in the second order polynomial structure (see Eq. (13)). Equating the exponentials with the same harmonic (exponentials with terms 0, $i\omega t$, $2i\omega t$) on both sides of the equation, a system of nonlinear equations for the unknown coefficients (Q_1, Q_{-1}, Q_2, Q_{-2}) is set. The resulting equations for the unknown coefficients are:

- Zeroth harmonic: $e^{0i\omega t}(\ldots\ldots) = 0$,

$$Q_0 - Q_0\sum_{l=1}^{N_Q} h_Q(l) - \frac{U_0^2}{4}\sum_{k=1}^{N_u}\sum_{m=1}^{N_u} h_{uu}(k,m)\left(e^{-i\omega(k-m)\Delta t} + e^{-i\omega(m-k)\Delta t}\right) - \sum_{k=1}^{N_u}\sum_{l=1}^{N_Q} h_{uQ}(k,l)\left(\frac{U_0 Q_{-1}}{4i}e^{-i\omega(k-1-l)\Delta t} - \frac{U_0 Q_1}{4i}e^{-i\omega(l-k+1)\Delta t}\right) = 0. \tag{23}$$

- First harmonic: $e^{i\omega t}(\ldots\ldots) = 0$,

$$Q_1 - \frac{U_0}{2i}\sum_{k=1}^{N_u} h_u(k)e^{-i\omega(k-1)\Delta t} - \frac{Q_1}{2}\sum_{l=1}^{N_Q} h_Q(l)e^{-i\omega l\Delta t} - \sum_{k=1}^{N_u}\sum_{l=1}^{N_Q} h_{uQ}(k,l)\left(\frac{U_0 Q_0}{2i}e^{-i\omega(k-1)\Delta t} - \frac{U_0 Q_2}{4i}e^{-i\omega(-k+1+2l)\Delta t}\right) = 0. \tag{24}$$

- Second harmonic: $e^{2i\omega t}(\ldots\ldots) = 0$,

$$\frac{Q_2}{2} - \frac{Q_2}{2}\sum_{l=1}^{N_Q} h_Q(l)e^{-2i\omega l\Delta t} + \frac{U_0^2}{4}\sum_{k=1}^{N_u}\sum_{m=1}^{N_u} h_{uu}(k,m)e^{-i\omega(k+m-2)\Delta t} - \frac{U_1 Q_1}{4i}\sum_{k=1}^{N_u}\sum_{l=1}^{N_Q} h_{uQ}(k,l)e^{-i\omega(k+l-1)\Delta t} = 0. \tag{25}$$

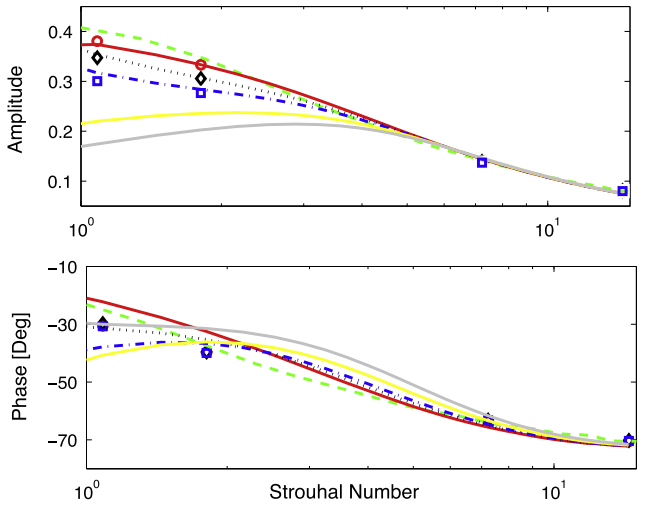

Fig. 12. Gain and the phase of the transfer function obtained with single harmonic forcing, second order identification and linear identification on a semi-logarithmic plot. NL Ident (red – 0.30, dotted black – 0.75, dash-dotted blue – 1, yellow – 1.5, gray – 2), green-Linear Identification, Single Harmonic Forcing (Markers, same color). (For interpretation of the references to color in this figure legend, the reader is referred to the web version of this article.)

The system of equations is included for the complex conjugate parts. Although this step is not necessary, it is useful to check if the resulting coefficients indeed are complex conjugate. This algebraic system of equations for the coefficients of the harmonic ansatz is solved with a nonlinear solver which uses Levenberg–Marquardt algorithm. For the present case, inclusion of third and fourth harmonics has negligible influence on the solution, whereas addition of five or more harmonics results in inaccurate results or the solution for the nonlinear system of equations does not converge. In Fig. 12, the results for the amplitude and phase of the transfer function at the forcing frequency are shown.

The comparison of the nonlinear transfer function from single harmonic forcing and harmonic balancing of the second order identification shows good agreement for the gain up to $A = 1$, where the nonlinear effect is already noticable as a decrease in the gain of the transfer function. The agreement in the gain deteriorates at low Str for $A = 1.5$ and $A = 2$. The deviation for the phase is even stronger. But the phase has a negligible amplitude dependence nonlinearity up to $A = 1.5$, which has been shown earlier when deriving the nonlinear transfer function from FFT. One can also consider a polynomial order of higher degree (3rd order, 4th order, etc.). In this case, nonlinearity in the low frequency ranges will be captured better. However, the number of the terms in the harmonic balance equations will be increased which may be a problem when solving the nonlinear system of equations for the coefficients of the harmonic ansatz.

5.3.5. Harmonic probing

A wide class of nonlinear systems is expressed as Volterra series representation [6,24]. This is the extension of the impulse response of a linear system into higher dimensions. The transfer function of a linear system is calculated by transforming the unit impulses into frequency domain (z-transform for a discrete case). The same analogy is used to define the higher order transfer functions of the nonlinear system by extension of the higher order impulses (Volterra kernels) into frequency domain. In the following sections, the higher order transfer functions are computed using second order polynomial identification derived earlier, and harmonic probing approach as by Bedrosian et al. [3].

The response of a nonlinear system is represented by Volterra series approximation as;

$$Q(t) = \underbrace{\int_{-\infty}^{\infty} h_1(\tau_1)u(t-\tau_1)\,d\tau_1}_{\text{Impulse response}} + \int_{-\infty}^{\infty}\cdots\int_{-\infty}^{\infty}\underbrace{h_n(\tau_1,\ldots,\tau_n)}_{n\text{th order kernel}}u(t-\tau_1)\cdots u(t-\tau_n)d\tau_1\cdots d\tau_n+\cdots. \tag{26}$$

The extension of the higher order Volterra kernels in the frequency domain gives the higher order transfer functions [3]. The first order or linear transfer function is defined as,

$$H_1(\omega) = \int_{-\infty}^{\infty} h_1(\tau_1)e^{-i\omega\tau_1}\,d\tau_1, \tag{27}$$

and similar definitions apply for the other kernels. The nth order transfer function is defined as,

$$H_n\left(\underbrace{\omega_1,\ldots,\omega_n}_{\omega_1+\ldots+\omega_n=\omega}\right) = \int_{-\infty}^{\infty}\cdots\int_{-\infty}^{\infty} h_n(\tau_1,\ldots,\tau_n)e^{-i\omega_1\tau_1\cdots-i\omega_n\tau_n}\,d\tau_1\cdots d\tau_n. \tag{28}$$

The input spectra at a specific frequency could produce terms which can be multiple integer frequencies, and inter modulations which are specific to nonlinear systems. The higher order transfer functions take these effects into account [22,54]. The computation of higher order transfer functions is performed by harmonic probing method as by Bedrosian et al. [3]. A schematic representation of the approach to find the higher order transfer functions is shown in Fig. 13.

To find the first order transfer function, the system is excited with single harmonic forcing,

$$u(t) = e^{i\omega t}, \tag{29}$$

and the corresponding response calculated from Volterra series representation is given as,

$$Q(t) = H_1(\omega)e^{i\omega t} + H_2(\omega,\omega)e^{2i\omega t} + H_3(\omega,\omega,\omega)e^{3i\omega t}. \tag{30}$$

The input (Eq. (29)) and output (Eq. (30)) are then used in the second order polynomial identification (Eq. (13)). Taking only the linear terms in the response and equating the terms of the first order exponentials, the linear transfer function is obtained as,

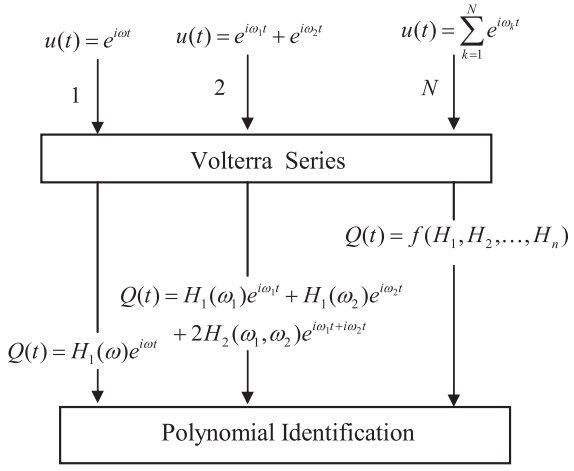

Fig. 13. Schematic of the harmonic probing method to find the higher order transfer functions.

$$H_1(\omega) = \frac{\sum_{k=1}^{N_u} h_u(k) e^{-i(k-1)\omega\Delta t}}{1 - \sum_{l=1}^{N_Q} h_Q(n) e^{-il\omega\Delta t}}. \quad (31)$$

The computation of the second order transfer function requires harmonic forcing at two different frequencies [3,7],

$$u(t) = e^{i\omega_1 t} + e^{i\omega_2 t}. \quad (32)$$

The corresponding nonlinear response is obtained from Volterra series representation as,

$$Q(t) = H_1(\omega_1)e^{i\omega_1 t} + H_1(\omega_2)e^{i\omega_2 t} + 2H_2(\omega_1,\omega_2)e^{i\omega_1 t + i\omega_2 t}. \quad (33)$$

Again, this response is used in the polynomial identification structure in Eq. (13), and the terms of exponentials which correspond to the sum of the frequencies are equated to find the second order transfer function as,

$$H_2(\omega_1,\omega_2) = \frac{\begin{pmatrix} \sum_{k=1}^{N_u}\sum_{m=1}^{N_u} h_{uu}(k,m)(e^{-i(k-1)\omega_1\Delta t} + e^{-i(m-1)\omega_1\Delta t}) \\ +\sum_{k=1}^{N_u}\sum_{l=1}^{N_Q} h_{uQ}(k,l)H_1(\omega_1)e^{-i(k-1)\omega_2\Delta t - il\omega_1\Delta t} \\ +\sum_{k=1}^{N_u}\sum_{l=1}^{N_Q} h_{uQ}(k,l)H_1(\omega_2)e^{-i(k-1)\omega_1\Delta t - il\omega_2\Delta t} \end{pmatrix}}{2 - 2\sum_{l=1}^{N_Q} h_Q(l)e^{-il\omega\Delta t}}. \quad (34)$$

The computation of the third order transfer function requires excitation at three different frequencies. The computation of higher order transfer functions is straightforward using this method, once the coefficients of the polynomial identification are obtained with unsteady CFD and broadband forcing. The higher order transfer functions are then computed as the functions of frequency and the coefficients. The relation is recursive as also seen from Eq. (34). Although the procedure to compute the higher order transfer functions with this approach is time consuming, generally a small number of higher order transfer functions are sufficient to achieve convergence in the response.

In Fig. 14, the responses from the single harmonic forcing, at $A = 0.3$, and linear identification are compared with the first order transfer function computed from harmonic probing. The overall agreement between the different methods is good for both phase and gain. In Fig. 15, the gain of the second order transfer function is shown. It is a surface plotted over two Str values, and highest values are achieved on the main diagonal. In Fig. 16, the gain of the first three transfer functions is shown. The amplitude of the third order transfer function on the main diagonal is much less than the first order transfer function.

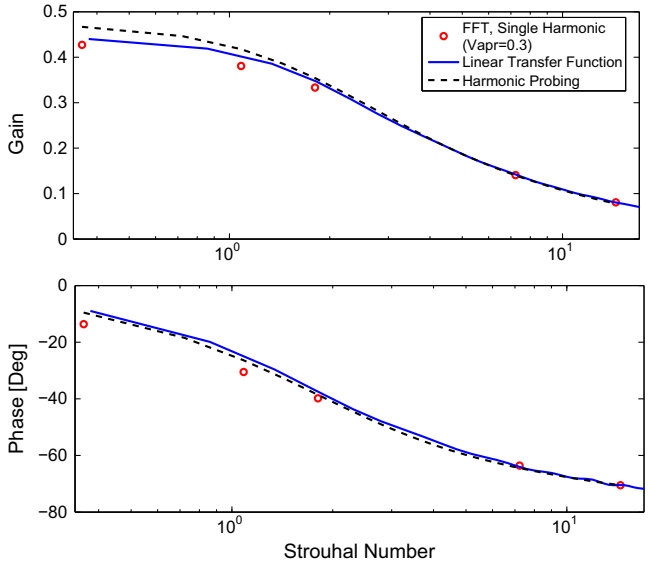

Fig. 14. Gain and the phase of the first order transfer function calculated from single sinusoid forcing at $A = 0.3$, linear system identification and harmonic probing on a semi-logarithmic plot.

5.4. Nonlinear black box identification

Nonlinear black box identification methods are promising besides the neural network to identify any nonlinearity up to a specified degree of accuracy [49]. For highly nonlinear systems black box identification can be used if little or no a priori information about the complex physics is available. Again in this case, one can utilize either the actual outputs or computed outputs from the model in the regressor set. In the former case with a small number of regressors, highly accurate results can be obtained even though the identification procedure leads to a nonlinear optimization problem. For our purposes, this may not seem to be a good choice since at each time we require output from CFD (actual outputs). But an extension of this identification in the frequency domain is possible and the accuracy is better than a polynomial identification we considered before. In the following, we present the equations for the nonlinear black box identification, validate the results against single harmonics, compare it with the polynomial identification and later discuss about the extension into the frequency domain.

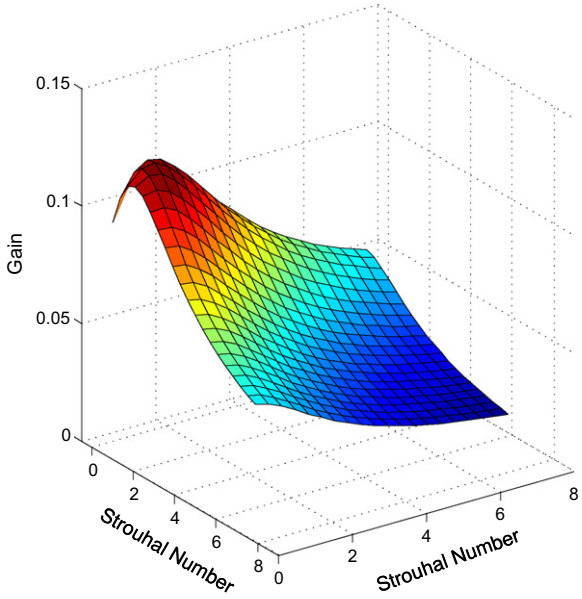

Fig. 15. Gain of the second order transfer function computed from the recursive relation of the harmonic probing approach.

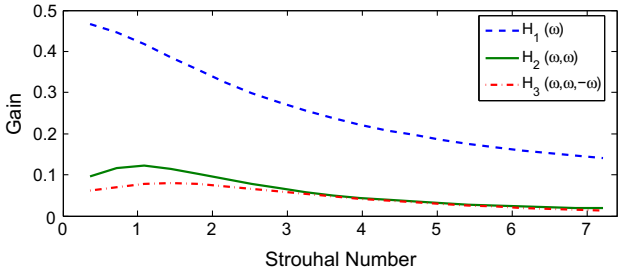

Fig. 16. Gain of the first three transfer functions on the main diagonal computed from the recursive relation of the harmonic probing approach.

5.4.1. Mathematical formulation

From a measured input output data set, a dynamical model will be constructed. The procedure consists of three steps:

- The numbers of the past inputs N_u and outputs N_Q ("regressors") are selected. The model structures that could be used are nonlinear extension of linear model structures, e.g. NARX, NFIR, and NOE.
- From the space of regressors to the nonlinear response, a nonlinear map will be created using functional expansions like wavelet, sigmoid units.
- The criterion to minimize the difference between the actual output and output from identification will result in a nonlinear least square fit. Optimization techniques like Gauss–Newton or Levenberg–Marquardt can be used to find the parameters of nonlinearity.

The method offers a lot of flexibility in usage and construction of different dynamic fits. On the other hand, the number of significant parameters and the well-known problems of nonlinear least square minimization – optimum initial values, local minima, etc. – are disadvantages of the method [49]. The output consists of a linear and a nonlinear part,

$$Q(t) = \widetilde{Q}_L(t) + \sum_{i=1}^{N} \alpha_i f\left(\beta_i^T \varphi + \gamma_i\right), \tag{35}$$

where φ, y are the vector of regressors and output, α, β and γ the parameters of nonlinearity, N the number of units. The nonlinear block consists of units that have parameters of nonlinearity and expansion functions like wavelets or sigmoids. Choosing the appropriate regressors are important otherwise the structure will results in a significant number of parameters.

5.4.2. Nonlinear black box identification of localized heat source

As the input, again a broadband forcing of velocity amplitude ratio $A = 2$ is applied at the inlet as before for the second order identification procedure. The approximated output is a general function of past inputs and outputs,

$$\widetilde{Q}(t) = F(Q(t-1), \ldots, Q(t-N_Q), u(t), \ldots, u(t-N_U)). \tag{36}$$

The space of regressors consists of the following terms,

$$[u(t),\ u(t-1),\ u(t-2),\ Q(t-1),\quad Q(t-2),\ Q(t-3),\ Q(t-4)].$$

The next step to consider is the number of units and the approximation functions in the nonlinear unit. The number of units is 4. Increasing the number of units does not improve the accuracy and moreover may lead to an over-parametrization. A linear block along with the nonlinear block is also added. For nonlinear optimization, the Levenberg–Marquardt method is used. Half of the time series data is used for estimation, while the other is used for validation. Validation is also performed for single harmonic excitations at different Strouhal numbers and velocity amplitude ratios. First a wave like function, see Fig. 17 below, is used as an approximator in the nonlinear unit. The results using this function as approximator have globally good behavior. However, the local behavior was found to have oscillatory behavior. Therefore, in the nonlinear unit a combination of both sigmoid and wavelet are used as approximation functions. The model structure, the regressors and the number of units is the same as before.

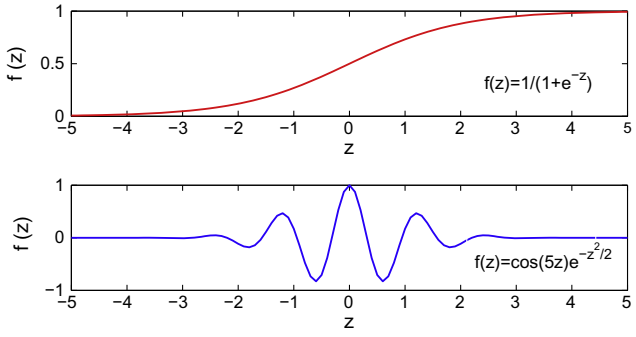

Fig. 17. Approximation functions used in the nonlinear unit, Sigmoid (above), Wavelet (below).

The degree of fit to the validation data (for the unused part of the broadband forcing) is 99.5. Once the coefficients of the functional expansion representation in Eq. (34) are computed, they will be used to validate the results against single harmonic forcing, see Tables 2 and 3. The increase in performance with nonlinear black box identification compared to the second order polynomial identification can be seen clearly from the percentage in the error for the second harmonic in Table 3. It is always less than 1.6 %. It is clearly seen that nonlinear black box identification has better accuracy compared to the polynomial identification especially for the second harmonic. But for our purposes at each time CFD data are required ("actual outputs"). As mentioned before the advantages of these methods can be used when extending them into the frequency domain, otherwise they are useless for our purposes. In the next, we consider the extension of the nonlinear black box identification into the frequency domain.

5.4.3. Higher order transfer functions for nonlinear black box identification

The higher order transfer functions can also be computed from the nonlinear black box structure [7]. The method is the same as for computation of the transfer functions from the second order polynomial identification. The functional representation can be expanded into a Taylor series representation around the constant term in the functional (see nonlinear part of the Eq. (34)) as,

$$Q_{NL}(t) = \sum_{k=1}^{N} \sum_{n=0}^{\infty} \alpha_k \frac{f^{(n)}(\gamma_k)}{n!} \left(\beta_k^T \varphi\right)^n. \tag{37}$$

Table 2
Error in percentage for the fundamental harmonic with CFD, second order polynomial identification and nonlinear black box identification. SO: Second order polynomial identification. NBB: Nonlinear black box identification.

Strouhal number	Velocity amplitude ratio					
	1		1.5		2	
	SO	NBB	SO	NBB	SO	NBB
0.36	0.11	0.08	0.06	0.60	0.47	1.23
1.81	0.36	0.07	0.51	0.16	0.79	0.56
7.23	0.07	0.07	0.15	0.001	0.45	0.04

Table 3
Error in percentage for the second harmonic with CFD, second order polynomial identification and nonlinear black box identification. SO: Second order identification. NBB: Nonlinear black box identification.

Strouhal number	Velocity amplitude ratio					
	1		1.5		2	
	SO	NBB	SO	NBB	SO	NBB
0.36	4.5	1.48	1.78	1.03	0.11	0.75
1.81	5.93	1.11	4.16	1.01	2.35	0.80
7.23	12.4	0.72	10.5	1.1	8.26	1.57

Or more explicitly,

$$Q_{NL}(t) = \sum_{k=1}^{N} \sum_{n=0}^{\infty} \alpha_k \frac{f^{(n)}(\gamma_k)}{n!} \left(\sum_{s=1}^{N_u} \beta_{ks}^{u} u(t-s+1) + \sum_{r=1}^{N_Q} \beta_{kr}^{Q} Q(t-r) \right)^n, \tag{38}$$

where $f^{(n)}$ represents the nth derivative of the function. β_{ks}^{u}, β_{kr}^{Q} represent the coefficients for input and output at delays s and r, unit k, respectively.

To determine the linear transfer function, harmonic probing method will be used and the terms in the functional expansions (Eq. (34)) that should be considered are only the terms associated with the first degree of the polynomial. The analytical form of the linear transfer function from the nonlinear black box identification is found as,

$$H_1(\omega) = \frac{\sum_{s=1}^{N_u} h_u(s) e^{-i\omega(s-1)\Delta t} + \sum_{k=1}^{N} \sum_{s=1}^{N_u} \alpha_k f^{(1)}(\gamma_k) \beta_{ks}^{u} e^{-i\omega(s-1)\Delta t}}{1 - \sum_{r=1}^{N_q} h_Q(r) e^{-i\omega r \Delta t} + \sum_{k=1}^{N} \sum_{r=1}^{N_q} \alpha_k f^{(1)}(\gamma_k) \beta_{kr}^{Q} e^{-i\omega r \Delta t}}. \tag{39}$$

Here, h_u and h_Q represent the coefficients from the linear block, and the other terms are as defined before.

To compute the second order transfer function, polynomial degrees up to second order should be considered. Polynomials can also be used in the nonlinear block as expansion functions in the nonlinear black box NARX model, and the validation results show better performances compared to the second order identification. One can also use directly the polynomial nonlinear black box structure to compute the higher order transfer functions and in that case there is no need to expand the functions in Taylor series representation.

6. Summary and conclusions

Various approaches of nonlinear system identification have been explored, with the aim of obtaining a nonlinear dynamic model of heat transfer in pulsating flow. The models are constructed using only input–output data – where "input" is a velocity perturbation, while "output" is the heat release rate – which are generated by unsteady CFD computation of the flow in the immediate vicinity of the heat source. This approach affords both accuracy and flexibility for the formulation of a nonlinear heat source model.

The nonlinear system identification problem is interpreted as a general nonlinear functional approximation (function of the past inputs and past outputs). In the first step of the identification, a suitable excitation signal (a broadband signal of high amplitude) is chosen in order to excite all modes and amplitudes of interest. A priori knowledge of the approximate time lag of the system is useful, but this information could be obtained as a black-box approach as well. The number of past inputs and outputs that should be retained in the model is then selected according to the time step of the simulation and the time lag of the system.

It is important to distinguish between thermoacoustic system models formulated in the time domain or the frequency domain, respectively. In the former case, equation error type model structures for the heat source are not useful, since they require actual outputs for the set of regressors. On the other hand, output error models, which make use of outputs predicted by the model, may lead to instability and typical problems of nonlinear optimization.

In this paper an equation error type model with the polynomials up to second order was considered first. The approach was extended into the frequency domain with two different approaches, which provide the nonlinear transfer function (the "describing function") as well as higher order transfer function of the heat source: a harmonic balance approach and a harmonic probing approach. In the former case, a system of equations for the coefficients of the harmonic ansatz, and in the latter case, a recursive relation to compute the higher order transfer functions is obtained. The latter approach is computationally inefficient if transfer functions with order higher than four are required. But generally, a few higher order transfer functions are sufficient to get convergence in the response.

The last identification method considered was nonlinear black box identification. Even though this identification leads to a nonlinear optimization problem, the accuracy achieved with this scheme is high compared to polynomial identification, especially capturing the second harmonics for the single harmonic excitations. An extension of this identification procedure in the frequency domain is also possible, using a Taylor series approximation around the bias parameter. Alternatively, one can use polynomials in the expansion function of the nonlinear block. In this case, an extension into the frequency domain is straightforward.

If the heat source is described in terms of higher order transfer functions, it is generally valid for a range of amplitudes and frequencies of the pulsating velocity. This then serves as a basis for thermoacoustic system modeling strategies with coupled modes in the frequency domain [46,47]. In the previous studies for modeling approaches of the full thermoacoustic systems, sinusoidal describing function was the only method considered, since an adequate representation of the nonlinear heat source in the frequency domain which allows coupling of the modes was not available. This heat source model can be used in the frequency domain, when the limit cycles are formed because of the nonlinearity in the transfer function and have higher harmonics which are at the multiple integers of the fundamental harmonic.

Acknowledgments

We thank Prof. R.I. Sujith from IIT Madras for helpful discussions. Financial support was provided by Deutsche Forschungsgemeinschaft (DFG Po 710/6) and the Department of Science and Technology (DST) of India.

References

[1] Babuska R. Fuzzy modeling for control. Boston: Kluwer Academic Publishers.; 1998.
[2] Babuska R, Verbruggen HB. Multiple model approaches to nonlinear modeling and control. London (UK): Taylor and Francis; 1997.
[3] Bedrosian E, Rice SO. The output properties of Volterra systems driven by harmonic and gaussian inputs. In: Proceedings of the IEEE; 1971.
[4] Billings SA. Identification of nonlinear systems – a survey. In: Proceedings of the IEEE; 1980.
[5] Boyd S, Chua LO. Fading memory and the problem of approximating nonlinear operators with Volterra series. IEEE Trans Circuits Syst 1985;32:1150–61.
[6] Boyd SP.Volterra series: engineering fundamentals. PhD thesis. Berkeley: University of California 1985.
[7] Chance JE, Worden K, Tomlinson GR. Frequency domain analysis of NARX neural networks. J Sound Vib 1998;213(5):915–41.
[8] Chen S, Billings SA. Neural networks for non- linear dynamic system modelling and identification. Int J Control 1992;56. 319n++346.
[9] Culick FEC. Non-linear growth and limiting amplitude of acoustic oscillations in combustion chambers. Combust Sci Technol 1971;3:1–16.
[10] Culick FEC. Unsteady motions in combustion chambers for propulsion systems. RTO-AG-AVT-039; 2006.
[11] Dowling AP. Nonlinear self-excited oscillations of a ducted flame. J Fluid Mech 1997;346:271–90.
[12] Dowling AP. The calculation of thermoacoustic oscillations. J Sound Vib 1995;180:557–81.
[13] Durox D, Schuller T, Noiray N, Candel S. Experimental analysis of nonlinear flame transfer functions for different flame geometries. Proc Combust Inst 2009;32(1):1391–8.
[14] Fluent Inc. FLUENT user's guide. Lebanon, NH; 2005.
[15] Föller S, Selimefendigil F, Polifke W., Linear identification of the unsteady heat transfer of a cylinder in pulsating crossflow. In: International conference on jets, wakes and separated flows; 2008.
[16] Gelb A, Velde WEV. Multiple-input describing functions and nonlinear system design. McGraw Hill; 1968.

[17] Hantschk C, Vortmeyer D. Numerical simulation of self-excited thermoacoustic instabilities in a Rijke tube. J Sound Vib 1999;3(277):511–22.
[18] Heckl A. Non-linear acoustic effects in the Rijke tube. Acustica 1990;72:63–71.
[19] King L. On the convection of heat from small cylinders in a stream of fluid: determination of the convection constants of small platinum wires with applications to hot-wire anemometry. Philos Trans Roy Soc 1914:373–432.
[20] Korenberg MJ, Bruder SB, McLlroy PJ. Exact orthogonal kernel estimation from finite data records: extending Wiener's identification of nonlinear systems. Ann Biomed Eng 1998;16:201–14.
[21] Korenberg MJ. Parallel cascade identification and kernel estimation for nonlinear systems. Ann Biomed Eng 1991;19:429–55.
[22] Lang ZQ, Billing SA. Energy transfer properties of nonlinear systems in the frequency domain. Int J Control 2005;78:345–62.
[23] Lee YW, Schetzen M. Measurement of the wiener kernels of a non-linear system by cross-correlation. Int J Control 1965;2(3):237–54.
[24] Li LM, Billings SA. Discrete time subharmonic modelling and analysis. Int J Control 2005;78(16):1265–84.
[25] Lieuwen T. Experimental investigation of limit-cycle oscillations in an unstable gas turbine combustor. J Propul Power 2002;18(1):61–7.
[26] Lighthill MJ. The response of laminar skin friction and heat transfer to fluctuations in the stream velocity. Proc Roy Soc A 1954;224:1–23.
[27] Lin CC. The theory of hydrodynamic stability. Cambridge Univ. Press; 1955.
[28] Ljung L. System identification: theory for the user. 2nd ed. Englewood Cliffs, New Jersey: Prentice Hall; 1998.
[29] Matveev KI. Energy consideration of the nonlinear effects in a Rijke tube. J Fluids Struct 2003;18(6):783–94.
[30] McManus KR, Poinsot T, Candel SM. A review of active control of combustion instabilities. J Prog Energy Combust Sci 1993;19:1–29.
[31] Narendra K, Parthasarathy K. Identification and control of dynamical systems using neural networks. IEEE Trans Neural Networks 1990;1:4–27.
[32] Nicoud F, Benoit L, Sensiau C, Poinsot T. Acoustic modes in combustors with complex impedances and multidimensional active flames. AIAA J 2007;45(2):426–41.
[33] Noiray N, Durox D, Schuller T, Candel S. A unified framework for nonlinear combustion instability analysis based on the flame describing function. J Fluid Mech 2008;615:139–67.
[34] Nørgaard M, Ravn O, Poulsen NK. Nnsysid-toolbox for system identification with neural networks. mathematical and computer modelling of dynamical systems. Math Comput Model Dynam Syst 2002;8(1):1–20.
[35] Nowak RD. Nonlinear system identification. Circuits Syst Signal Process 2002;21:109–22.
[36] Pankiewitz C, Sattelmayer T. Time domain simulation of combustion instabilities in annular combustors. Trans ASME – J Eng Gas Turbines Power 2003:677–85.
[37] Paparizos LG, Culick FEC. The two-mode approximation to nonlinear acoustics in combustion chambers. I. Exact solution for second order acoustics. Combust Sci Technol 1989;65(1):39–65.
[38] Pha DT. Neural networks for identification, prediction and control. Springer; 1995.
[39] Polifke W. Combustion instabilities. In: Anthoine J, Hirschberg A, editors, Advances in aeroacoustics and applications. VKI LS 2004-05. Rhode-St-Genèse (BE): Von Karman Institute, March 15–19, 2004.
[40] Polifke W. Numerical techniques for identification of acoustic multi-poles. In: Advances in aeroacoustics and applications. VKI LS 2004-05. Brussels (BE) Von Karman Institute: March 15–19, 2004.
[41] Polifke W. System identification for aero- and thermo-acoustic applications. In: Schram C, editor, Advances in aero-acoustics and thermo-acoustics. VKI LS 2011-01. Rhode-St-Genèse (BE): Von Karman Institute; 2011. ISBN:13 978-2-87516-012-6.
[42] Polifke W, Gentemann AM. Order and realizability of impulse response filters for accurate identification of acoustic multi-ports from transient CFD. J Acoust Vib 2004;9(3):139–48.
[43] Polifke W, Poncet A, Paschereit CO, Döbbeling K. Reconstruction of acoustic transfer matrices by instationary computational fluid dynamics. J Sound Vib 2001;245:483–510.
[44] Rugh WJ. Nonlinear system theory. The Johns Hopkins University Press; 1981.
[45] Schuller T, Ducruix S, Durox D, Candel S. Modeling tools for the prediction of premixed flame transfer functions. Proc Combust Inst 2002;29(1):107–13.
[46] Selimefendigil F, Polifke W. A frequency domain system model with coupled modes for limit cycle prediction of thermoacoustic systems. Int J Spray Comb Dynamics 2011;3(3&4):303–30.
[47] Selimefendigil F. Identification and analysis of nonlinear heat sources in thermo-acoustic systems. PhD thesis. TU München; 2010.
[48] Shreekrishna, Hemchandra Santosh, Lieuwen Tim. Premixed flame response to equivalence ratio perturbations. Combust Theory Model 2010;14(5): 681–714.
[49] Sjöberg J, Zhang Q, Ljung L, Benveniste A, Delyon B, Glorennec PY, et al. Nonlinear black-box modeling in system identification: a unified overview. Automatica 1995;31(12):691–1724.
[50] Söderström T, Stoica P. System identification. Hemel Hempstead (UK): Prentice-Hall International; 1989.
[51] Takagi T, Sugeno M. Fuzzy identification of systems and its application to modeling and control. IEEE Trans Syst Man Cyber 1985;15(1):116–32.
[52] Telionis D. Unsteady viscous flows. Springer; 1981.
[53] Veynante D, Poinsot T. Theoretical and numerical combustion. R.T. Edwards, Inc.; 2005.
[54] Wu XF, Lang ZQ, Billings SA. Analysis of the output frequencies of nonlinear systems. IEEE Trans Signal Process 2007;55:3239–46.
[55] Yang V, Kim SI, Culick FEC. Triggering of longitudinal pressure oscillations in combustion chambers. I: Nonlinear gasdynamics. Combust Sci Technol 1990;72(4):183–214.
[56] Zinn BT, Lores ME. Application of the Galerkin method in the solution of nonlinear axial combustion instability problems in liquid rockets. Combust Sci Technol 1971;14:269–78.